3*d* transition metal impurities in diamond: Electronic properties and chemical trends

L. V. C. Assali,[1] W. V. M. Machado,[1] and J. F. Justo[2]
[1]*Instituto de Física, Universidade de São Paulo, CP 66318, CEP 05315-970, São Paulo, SP, Brazil*
[2]*Escola Politécnica, Universidade de São Paulo, CP 61548, CEP 05424-970, São Paulo, SP, Brazil*
(Received 2 June 2011; revised manuscript received 20 July 2011; published 17 October 2011)

First principles calculations have been used to investigate the trends on the properties of isolated 3*d* transition metal impurities (from Sc to Cu) in diamond. Those impurities have small formation energies in the substitutional or double semivacancy sites and large energies in the interstitial site. Going from Sc to Cu, the 3*d*-related energy levels in the band gap move from the top of the band gap toward the valence band in all three sites. Trends in electronic properties and transition energies of the impurities, in the substitutional or interstitial sites, are well described by a simple microscopic model considering the electronic occupation of the 3*d*-related levels. On the other hand, for the impurities in the double semivacancy site, there is a weak interaction between the divacancy- and the 3*d*-related orbitals, resulting in vacancy- and 3*d*-related levels in the materials band gap.

DOI: 10.1103/PhysRevB.84.155205 PACS number(s): 61.72.Bb, 71.55.Cn

I. INTRODUCTION

Silicon-based device technology has flourished over the last four decades. In such a time span, miniaturization was the keyword for improving device performance. When new challenges were foreseen in the horizon, designers used to find new solutions to overcome them.[1] In a near future, intrinsic physical limits of this technology may preclude further improvements.[2] A different route for electronic devices could be the use of wide band gap semiconductors,[3] since, when compared to silicon, they present superior materials properties for electronic devices, such as larger thermal conductivity, dielectric strength, and electron saturation velocity. There are still several technical limitations that prevent their competitiveness with the well-established silicon technology. However, those materials have found their niche over the last decade, with applications in specific areas such as high-power, high-temperature, high-frequency, optoelectronic,[4,5] and spintronic[6,7] devices.

There is currently a high demand for devices to operate under extreme conditions, and diamond is one of the leading candidates for such applications.[8–10] This material has a wide band gap (experimental value of 5.5 eV), high saturated carrier velocities, high electric field breakdown strength, low dielectric constant, and high thermal conductivity. Synthetic diamond has been grown out of graphite by high pressure–high temperature methods for about fifty years,[11] being currently the most widely used growing process for obtaining macroscopic diamond samples. In those processes, 3*d* transition metal (TM) alloys, involving mainly nickel, cobalt, and iron, are used as solvent-catalysts to both overcome the sp^2 to sp^3 energy barrier and accelerate the growth process.[12] Those TM end up being incorporated in the resulting diamond as residual impurities, either in isolated configurations or forming complexes with other defects that can generate electrically and optically active centers.[12,13] Several transition metal-related active centers have been experimentally identified in diamond and have been associated with impurities in substitutional, interstitial, or double semivacancy configurations.[13–16] Understanding the nature and microscopic structure of those centers is crucial in developing diamond-related technologies.

Here we used first principles total energy calculations to investigate the electronic properties and chemical trends of 3*d* TM-related centers (from Sc to Cu) in diamond. We focused on the trends of impurities in the substitutional, interstitial, or double semivacancy sites. The stability of those defects, in all three sites, were computed in terms of their formation energies. The electronic structure of this $3d^n$ impurity family shows clear chemical trends in any site, with the 3*d*-related levels deepening from the top of the gap toward the valence band with increasing number (n) of 3*d* electrons. Additionally, we show that the respective electronic properties and transition energies could only be rationalized in terms of the number of electrons occupying the 3*d*-related energy levels within the materials band gap.

II. METHODOLOGY

The calculations were carried using the all-electron spin-polarized full-potential linearized augmented plane wave (FP-LAPW) method[17] implemented in the WIEN2K package.[18] The electron-electron interactions were described within the framework of the density functional theory and the generalized gradient approximation.[19] Calculations were performed considering a 54-atom reference face-centered cubic (FCC) supercell and a Monkhorst-Pack ($2 \times 2 \times 2$) grid to sample the irreducible Brillouin zone.[20] Convergence on the total energy was achieved using a plane wave basis set to describe the interstitial region, with the set limited by the wave number $7.0/R$, where $R = 1.2$ a.u. (0.635 Å) is the radius of all atomic spheres. Self-consistent iterations were performed until convergence on the total energy of 10^{-4} Ry was achieved. In all systems with impurities, the internal degrees of freedom were optimized, without any symmetry constraints, until the force in each atom was smaller than 10^{-3} Ry/a.u. Such theoretical framework and convergence criteria have been shown to provide a reliable description of the electronic properties of defect centers in several semiconductors.[21,22]

The formation energy of a TM impurity center in diamond (E_f^q) was computed by[13,23]

$$E_f^q = E_{\text{tot}}^q(N_C, N_{TM}) - N_C\mu_C - N_{TM}\mu_{TM} + q(\varepsilon_v' + \epsilon_F), \quad (1)$$

where $E^q_{\rm tot}(N_{\rm C}, N_{TM})$ is the total energy of a supercell with the defect in a q charge state, with $N_{\rm C}$ carbon atoms and N_{TM} TM impurity atoms. The $\mu_{\rm C}$ and μ_{TM} are the chemical potentials of diamond and TM stable crystalline structures, respectively, computed within the same methodology described in the previous paragraph. Additionally, ϵ_F is the Fermi energy ($0 \leqslant \epsilon_F \leqslant \varepsilon_g$, where ε_g is the band gap energy) and $\varepsilon'_v = \varepsilon_v + \delta_q$, where $\delta_{\rm q}$ is a parameter that lines up the band structures of the bulk diamond material with and without the impurity in relation to the top of the valence band of pure crystal (ε_v). This correction in the valence band top (δ_q) is necessary due to inhomogeneities in the charge density in the finite primitive cell, which causes a Coulomb multipole interaction with its images, as discussed in Ref. 24. Additionally, a uniform jellium background was implicitly considered to cancel out the long-range multipole interactions of charged supercells.[23]

For a certain impurity (in a substitutional, interstitial, or double semivacancy center), the transition energy between the q' and q charge states, $E_t(q'/q)$, is the value of the Fermi energy in the band gap when the formation energies of the center in those respective charge states, as computed by Eq. (1), are equal:

$$E_t(q'/q) = \epsilon_F \quad \text{when} \quad E^{q'}_f - E^q_f = 0. \tag{2}$$

Within our theoretical approximations, we found $\varepsilon_g = 4.56$ eV for diamond. This theoretical gap value is smaller than the experimental one of 5.42 eV for $T = 100$ K.[25] It is well documented in the literature that the density functional theory generally underestimates the materials band gap value, although it provides an appropriate description on the ground state of any electronic system, as well as on the position of the transition states in the gap material, as discussed in Ref. 26. We should stress that here we computed the transition energies, not the excitation ones, in which other methodologies could be more appropriate.[27]

III. RESULTS AND DISCUSSION

We computed the properties of the $3d$ transition metal impurities in diamond, from Sc (atomic configuration $3d^1 4s^2$) to Cu (atomic configuration $3d^{10} 4s^1$), in three different sites: tetrahedral interstitial ($\rm TM_i$), substitutional ($\rm TM_s$), and double semivacancy ($\rm TM_{2V}$) ones.

When a TM impurity, with a $3d^n 4s^2$ ($1 \leqslant n < 9$) atomic configuration, occupies a tetrahedral interstitial site in diamond ($\rm TM_i$), its $4s$ electrons are transferred to the $3d$ orbitals, resulting in a $3d^{n+2}$ configuration. In a tetrahedral crystal field the $3d$ states are split into $e + t_2$ irreducible representations, with the threefold t_2 states lying lower in energy than the twofold e ones. This level ordering is the result of a strong octahedral crystal field created by the next nearest neighboring carbon atoms, which leads to a strong repulsion in the e states, moving them up to the upper half of the band gap. Additionally, the crystal field energy splitting ($\Delta^{\rm i}_{\rm CF}$) is larger than the exchange splittings ($\Delta^{\rm i}_{\rm e}$ and $\Delta^{\rm i}_{\rm t}$), such that the system always presents a low-spin configuration. This results from the small lattice parameter of diamond and is consistent with TM impurities in boron nitride.[28] Figure 1(a) presents the specific case of $\rm Mn_i$ in the neutral charge state ($3d^7$). For other $\rm TM_i$ impurities in diamond (from Sc to Cu), their t_2 and e levels have an equivalent behavior to those of $\rm Mn_i$, but with a chemical trend such that those levels move all together from the midgap region, in $\rm Sc_i$, toward the valence band, in $\rm Cu_i$, consistent with results for $\rm TM_i$ impurities in other semiconductors.[29,30] The $3d$ character localization in the TM atomic spheres increases with increasing the atomic number.

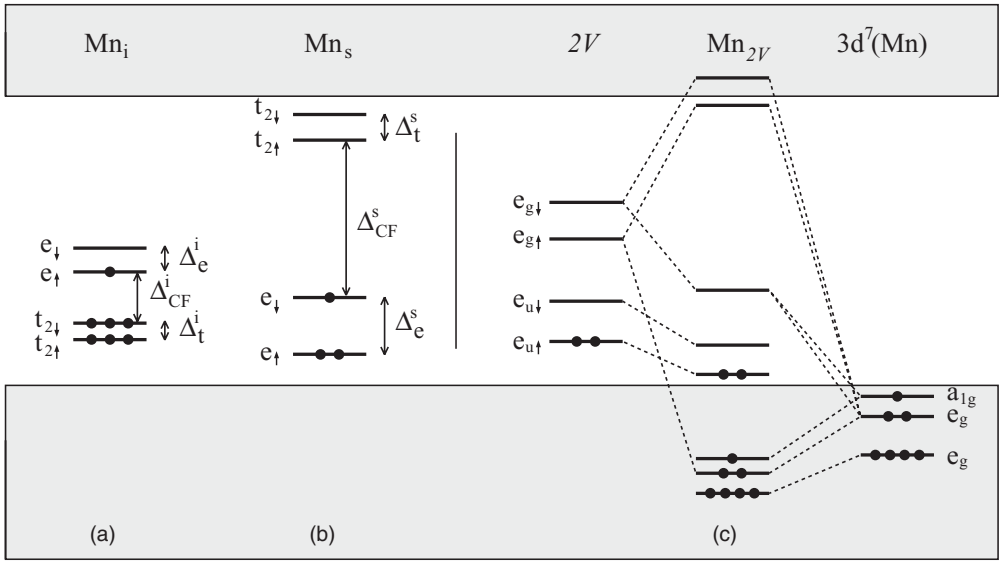

FIG. 1. Schematic representation of the gap energy electronic states for a manganese impurity in (a) interstitial ($\rm Mn_i$), (b) substitutional ($\rm Mn_s$), and (c) double semivacancy ($\rm Mn_{2V}$) sites. In the case of ($\rm Mn_{2V}$), the figure presents the model of a hybridization between the divacancy states ($2V$) and the $3d$ electrons in an isolated atomic configuration (Mn). The ↑ and ↓ arrows represent the spin up and down, respectively. Gray regions represent the diamond valence and conduction bands. For simplicity, the systems are represented considering a tetrahedral symmetry, neglecting symmetry-lowering distortions. For $\rm Mn_i$ ($\rm Mn_s$), the figure presents the exchange potential splittings $\Delta^{\rm i}_{\rm e}$ and $\Delta^{\rm i}_{\rm t}$ ($\Delta^{\rm s}_{\rm e}$ and $\Delta^{\rm s}_{\rm t}$) and the crystal field splitting $\Delta^{\rm i}_{\rm CF}$ ($\Delta^{\rm s}_{\rm CF}$).

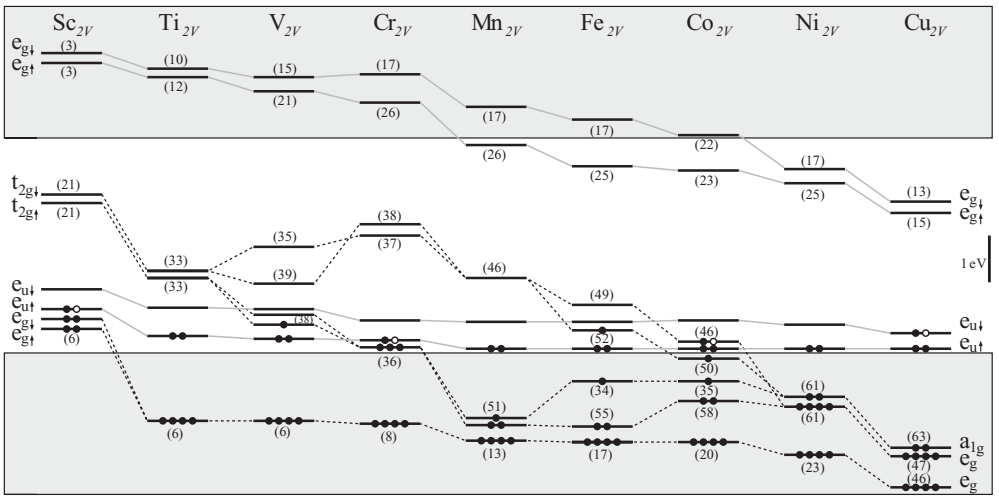

FIG. 2. The energy eigenvalues representing the divacancy- and TM 3d-related levels in the gap region for the TM_{2V} centers (TM = Sc, Ti, V, Cr, Mn, Fe, Co, Ni, and Cu). Levels with spin up and down are represented by ↑ and ↓ arrows, respectively. The filled (open) circles represent the electronic (hole) occupation of the gap levels. Numbers in parenthesis represent the d character percentage of charge inside the TM atomic spheres. Level labeling is consistent with the model presented in Fig. 1(c). For clarity, the results presented in the figure corresponded to a high-symmetry D_{3d} configuration, although the converged calculations took no symmetry constraints, as presented in Table I. Levels associated with the TM (divacancy) are connected by dashed (full gray) lines.

In the substitutional site (TM_s), the impurity presents a $3d^{n-2}$ configuration, since four electrons are necessary for a covalent bonding with the four nearest neighboring carbon atoms. In contrast to the interstitial case, the tetrahedral crystal field drives the e states to lie lower in energy than the t_2 ones. Here the crystal field splitting also prevails over the exchange splittings ($\Delta^s_{CF} \gg \Delta^s_t$ and Δ^s_e). Figure 1(b) presents the specific case of Mn_s in the neutral charge state ($3d^3$). For other TM_s impurities in diamond (from Sc to Cu), the e and t_2 levels are equivalent to those of Mn_s, but with a chemical trend such that those levels move all together from the band gap top, in Sc_s, toward the valence band, in Cu_s.[30] The 3d character localization in the TM atomic spheres also increases with increasing the atomic number.

The electronic structure of the TM impurity in the double semivacancy site (TM_{2V}) is considerably more complex than that in the other two sites. The electronic structure of TM_{2V} centers are the result of an interaction between the divacancy states with the ones coming from the atomic TM, as represented in Fig. 1(c) for the Mn_{2V} center. The one-electron ground state structure of a diamond divacancy in D_{3d} symmetry has the $e_u^2 e_g^0$ configuration in the band gap region. In that symmetry the TM 3d-related energy levels are split into $2e_g + a_{1g}$. When a TM atom is placed in the middle position of a divacancy, one of its e_g energy levels interacts slightly with the carbon dangling bonds, leaving a fully occupied nonbonding t_{2g}-like ($e_g + a_{1g}$) orbital inside the valence band. However, the other TM-related e_g orbital interacts with the divacancy-related e_g gap state, resulting in an e_g bonding level in the valence band and an e_g antibonding one in the band gap. The divacancy-related e_u orbitals do not interact with any 3d-related TM ones, and consequently they remain near the top of the valence band.

For the TM_{2V} center, depending on the impurity atomic number, the relative position of the 3d-related levels and the divacancy-related ones may switch along the series, such that the electronic structure of each impurity depends strongly on such relative positions and the center charge state. Figure 2 presents the electronic structure of the TM_{2V} in the neutral charge state. The figure presents, in parenthesis, the 3d character inside the TM atomic sphere of each energy level. Going from Sc_{2V} to Cu_{2V} impurity centers, the 3d-t_{2g}-related levels move from the middle of the band gap toward the valence band, crossing with the divacancy-related e_u levels that lie near the valence band top. Additionally, the percentage of d character increases along the series. These trends are consistent with those for substitutional and interstitial TM impurities. However, the electronic character of the highest occupied level of those centers depends on the relative position of the divacancy-related levels with respect to the 3d-related ones. According to Fig. 2, for the TM_{2V} in the neutral charge

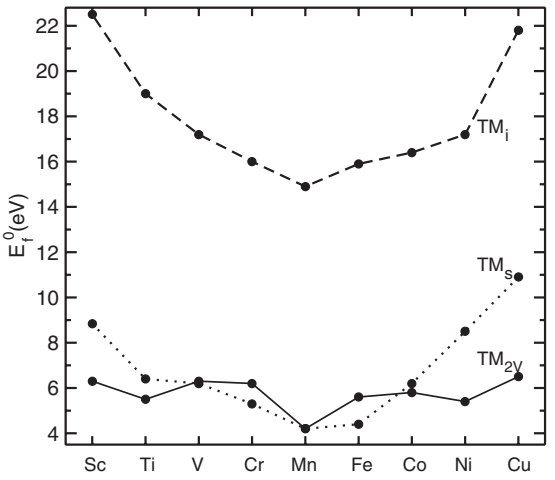

FIG. 3. Formation energy of the 3d TM impurities, in the neutral charge state (E_f^0), in substitutional (dotted line), interstitial (dashed line), and double semidivacancy (full line) sites.

TABLE I. Point symmetry and spin (S) for $3d$ TM impurities in the neutral charge state. The table presents results for interstitial, substitutional, and double semivacancy sites.

Site		Sc	Ti	V	Cr	Mn	Fe	Co	Ni	Cu
TM_i	Sym.	T_d	D_{2d}	D_2	T_d	D_{2d}	T_d	D_{2d}	T_d	D_{2d}
	S	3/2	0	1/2	0	1/2	1	1/2	0	1/2
TM_s	Sym.	D_{2d}	T_d	D_{2d}	T_d	D_{2d}	T_d	D_{2d}	C_1	T_d
	S	1/2	0	1/2	1	1/2	0	1/2	1	3/2
TM_{2V}	Sym.	C_{2h}	D_{3d}	D_{3d}	C_{2h}	D_{3d}	D_{3d}	C_{2h}	D_{3d}	C_i
	S	3/2	1	3/2	2	5/2	2	3/2	1	1/2

state, the highest occupied level is associated with the TM for V, Fe, and Co, while it is associated with the divacancy for Sc, Ti, Cr, Mn, Ni, and Cu.

Figure 3 presents the trends on the formation energy for neutral impurities in all three sites as computed by Eq. (1). The results show that the formation energies of a TM with $3d^n$ or $3d^{10-n}$ configurations are essentially equivalent in any site, with a clear energy favoring for the impurity in the middle of that family, which is manganese. Additionally, the interstitial site is the most unfavorable one for any TM, with formation energies more than 10 eV higher than the respective ones in the other two sites.[21] The small energy difference for the impurity in the substitutional or double semivacancy sites suggests that those two configurations may compete, coexisting in the diamond samples. We should also stress that trends in energy differences between TM defects in interstitial and substitutional configurations remain essentially the same for defects in charge states other than neutral. Those trends in energy are consistent, for example, with available experimental data for concentrations of cobalt[12] and nickel[13,16] impurities in as-grown and annealed synthetic diamond.

Table I presents the local symmetry and spin of the relaxed configuration for the TM impurities in the neutral charge state. As a result of the electronic structures, the TM_{2V} centers generally present spin values that are larger than the TM_i and TM_s centers. The manganese in the double semivacancy presents the largest spin of all centers ($S = 5/2$). This large spin value suggests potential applications for spintronic devices.[31,32]

Until now we have discussed the properties of the TM impurities in their neutral charge state. However, since those impurities introduce energy levels in the band gap, both occupied and unoccupied ones, there is often a large number of possible stable charge states for each center. The transition energy between two different charge states is important information for experimentalists to identify a certain center. Here we carried out calculations for all stable charge states of each TM impurity in those three sites. Some centers presented up to seven different stable charge states, with transition energies lying in the diamond band gap. The transition energy between two different charge states of a certain center was computed using the total energies of the centers in the initial and final charge states, as given by Eqs. (1) and (2).

Our results indicated that the chemical trends on transition energies [computed by Eq. (2)] along the $3d$ series could only be rationalized if they were discussed in terms of the $3d$-related level occupation and the respective crystal field and exchange splittings, as presented in Fig. 1. The comparison among different TM impurities should be conducted considering the same number of total electrons in each system, as discussed below. The transition energies within the diamond band gap for TM_s (from Sc to Cu) are shown in Fig. 4. The stable charge state of a certain center depends on the position of the Fermi level in the band gap. For example, the Ti_s presents two transition states in the band gap, the $(0/-)$ and $(-/2-)$, as shown in Fig. 4. This means that this center is stable in the neutral charge state for $0 < \epsilon_F \leqslant 3.0$ eV, in the negatively charge state for $3.0 \leqslant \epsilon_F \leqslant 3.8$ eV, and in the double negatively charge state for 3.8 eV $\leqslant \epsilon_F < \varepsilon_g$.

According to Fig. 1(b), the TM_s impurity centers introduce energy levels with e and t_2 irreducible representations, with $e_\uparrow$ and $e_\downarrow$ states below the $t_{2\uparrow}$ and $t_{2\downarrow}$ states. For an impurity with a $3d^n 4s^2$ atomic configuration, those levels are filled with $(n-2)d$ electrons. For the Sc_s^- center ($n = 2$), the e and t_2

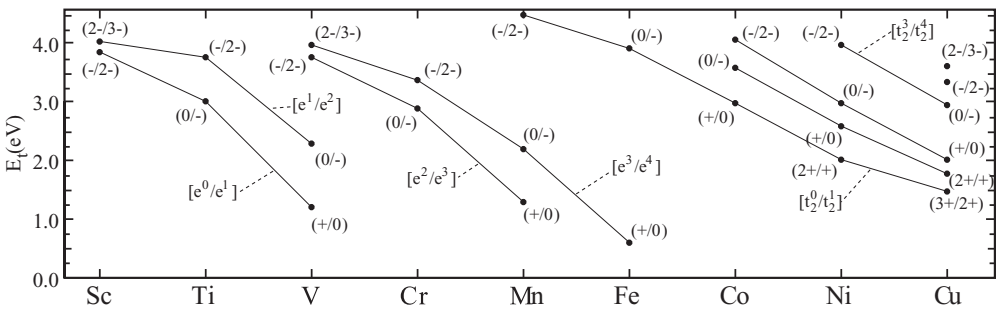

FIG. 4. Transition energies (E_t) of $3d$ TM impurities in the substitutional site. The initial and final $3d$-related band gap electronic configurations are given in square brackets (see text). The lines in the figure are only guides to the eye, connecting different transition states related with the same electronic configurations of different TM impurities.

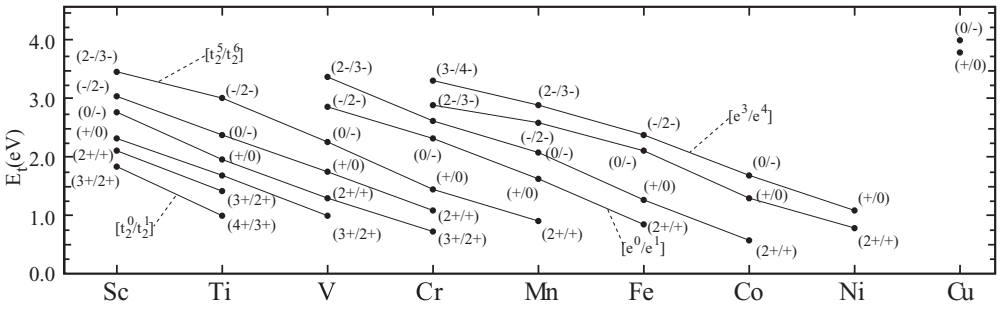

FIG. 5. Transition energies (E_t) of 3*d* TM impurities in the interstitial site. The lines and symbols are consistent with the ones in Fig. 4.

states are empty and the band gap electronic configuration is $e^0_\uparrow e^0_\downarrow t^0_{2\uparrow} t^0_{2\downarrow}$, where the level ordering is consistent with the increasing values of the respective energy eigenvalues, as given in Fig. 1(b). The Sc_s^{2-} center is related to adding one electron to an unoccupied e level, leading to the $e^1_\uparrow e^0_\downarrow t^0_{2\uparrow} t^0_{2\downarrow}$ band gap electronic configuration. Therefore, the $(-/2-)$ transition state is described by the connection between initial and final electronic configurations, as represented by $e^0_\uparrow e^0_\downarrow t^0_{2\uparrow} t^0_{2\downarrow} \rightarrow e^1_\uparrow e^0_\downarrow t^0_{2\uparrow} t^0_{2\downarrow}$. It could be represented in a compact form as $e^0 \rightarrow e^1$, or just $[e^0/e^1]$ in Fig. 4. Accordingly, the $(2-/3-)$ transition state, or $[e^1/e^2]$, is related to the $e^1 \rightarrow e^2$ electronic configurations. For Sc_s there is no additional transition state that lies in the band gap.

For Ti_s the $(0/-)$ and $(-/2-)$ transition states are associated with $e^0_\uparrow \rightarrow e^1_\uparrow$ and $e^1_\uparrow \rightarrow e^2_\uparrow$ electronic configurations, respectively. Those two transition states should be respectively compared to the $(-/2-)$ and $(2-/3-)$ transition states of the Sc_s center, which is why the transitions are connected by lines, as a guide to the eye, in Fig. 4. Going to V_s, the same electronic configurations are observed, being now related to the $(+/0)$ and $(0/-)$ transition energies. However, the V_s center carried two more possible electronic configurations in the diamond band gap, related to V_s^{2-} and V_s^{3-} centers, allowing computation of the transition energies between the electronic configurations $e^2_\uparrow e^0_\downarrow t^0_{2\uparrow} t^0_{2\downarrow} \rightarrow e^2_\uparrow e^1_\downarrow t^0_{2\uparrow} t^0_{2\downarrow}$ (or in a compact form, $e^2 \rightarrow e^3$) and $e^3 \rightarrow e^4$, associated with the $(-/2-)$ and $(2-/3-)$ transition states, respectively. The Mn_s impurity has four stable charge states in the band gap. For this impurity, after the $e_\uparrow$ and $e_\downarrow$ states are fully occupied, additional electrons could only occupy the t_2 states. For Mn_s there is the $e^4 t^0_{2\uparrow} t^0_{2\downarrow} \rightarrow e^4 t^1_{2\uparrow} t^0_{2\downarrow}$ transition associated with the $(-/2-)$ one. From Co_s to Cu_s, there are $e^4 t^0_{2\uparrow} t^0_{2\downarrow} \rightarrow e^4 t^1_{2\uparrow} t^0_{2\downarrow}$, $e^4 t^1_{2\uparrow} t^0_{2\downarrow} \rightarrow e^4 t^2_{2\uparrow} t^0_{2\downarrow}$, $e^4 t^2_{2\uparrow} t^0_{2\downarrow} \rightarrow e^4 t^3_{2\uparrow} t^0_{2\downarrow}$, and $e^4 t^3_{2\uparrow} t^0_{2\downarrow} \rightarrow e^4 t^3_{2\uparrow} t^1_{2\downarrow}$ (or $t_2^3 \rightarrow t_2^4$) transitions. Therefore one could associate, for example, the $(-/2-)$ transition of Sc_s with the $(0/-)$ one of Ti_s and the $(+/0)$ of V_s, i.e., transitions that involve the same number of electrons in the system. For all those centers it is observed that any transition state has a chemical trend to move from the top of the band gap in Sc toward the valence band maximum in Cu. Such a trend is the result of a Coulombic interaction, since the increasing atomic number, with a constant number of electrons, increases the nuclei-electron attractive interaction, reducing the total energy of the system.

Those results establish a microscopic model for a transition energy associated with the 3*d* level occupation in the band gap. There is a small energy difference between the $e^0 \rightarrow e^1$ and $e^1 \rightarrow e^2$ transitions, which is associated with the occupation of the $e_\uparrow$, being the result of a Coulombic interaction. There is a large energy difference between $e^1 \rightarrow e^2$ and $e^2 \rightarrow e^3$ transitions, which results from the exchange potential splitting (Δ_e^s). This is because the $e^2 \rightarrow e^3$ transition differs from the $e^1 \rightarrow e^2$ one by the addition of an electron with a different spin. The large energy difference between the $e^3 \rightarrow e^4$ and $t_2^0 \rightarrow t_2^1$ transitions results from the presence of a strong crystal field splitting (Δ_{CF}^s), which is larger than the exchange potential splittings (Δ_e^s and Δ_t^s). For the transitions related to the occupation of the $t_{2\uparrow}$ state (up to three electrons), the small energy difference is result of a Coulombic interaction. Finally, for the $t_2^3 \rightarrow t_2^4$ transition, the large energy difference is controlled by the exchange potential splitting of the t_2 state (Δ_t).

The same model could be used to discuss the transition energies associated with TM impurities in the interstitial site, as presented in Fig. 5. According to Fig. 1(a), the TM_i

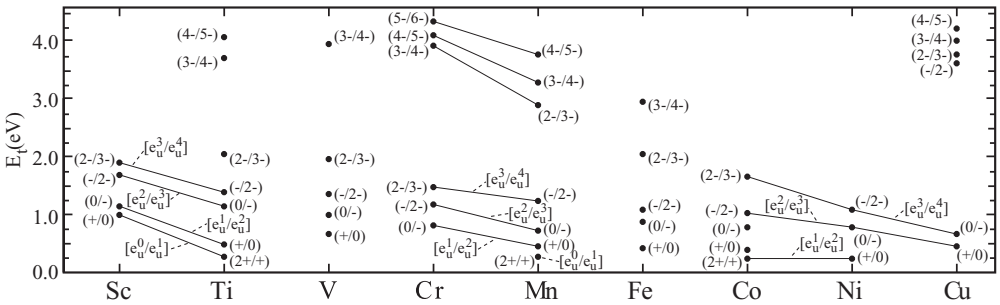

FIG. 6. Transition energies (E_t) of 3*d* TM impurities in the double semivacancy site. The lines and symbols are consistent with the ones in Fig. 4.

TABLE II. Electronic configuration (EC) for the divacancy-related and TM $3d$-related energy levels, and spin (S) for the TM^q_{2V} centers in diamond in q charge state, with TM = V, Fe,and Co.

	V_{2V}		Fe_{2V}		Co_{2V}	
q	EC	S	EC	S	EC	S
2+	——	—	——	—	$e^2_{g\uparrow}a^1_{1g\uparrow}a^1_{1g\downarrow}e^1_{u\uparrow}e^0_{g\downarrow}e^0_{u\downarrow}$	3/2
+	$e^2_{u\uparrow}a^0_{1g\uparrow}e^0_{g\uparrow}a^0_{1g\downarrow}e^0_{u\downarrow}e^0_{g\downarrow}$	1	$a^1_{1g\uparrow}e^2_{g\uparrow}e^2_{u\uparrow}a^0_{1g\downarrow}e^0_{g\downarrow}e^0_{u\downarrow}$	5/2	$e^2_{g\uparrow}a^1_{1g\uparrow}a^1_{1g\downarrow}e^2_{u\uparrow}e^0_{g\downarrow}e^0_{u\downarrow}$	2
0	$e^2_{u\uparrow}a^1_{1g\uparrow}e^0_{g\uparrow}e^0_{u\downarrow}e^0_{g\downarrow}a^0_{1g\downarrow}$	3/2	$e^2_{g\uparrow}a^1_{1g\uparrow}e^2_{u\uparrow}a^1_{1g\downarrow}e^0_{u\downarrow}e^0_{g\downarrow}$	2	$e^2_{g\uparrow}a^1_{1g\uparrow}a^1_{1g\downarrow}e^2_{u\uparrow}e^1_{g\downarrow}e^0_{u\downarrow}$	3/2
−	$e^2_{u\uparrow}a^1_{1g\uparrow}e^1_{u\downarrow}e^0_{g\uparrow}e^0_{g\downarrow}a^0_{1g\downarrow}$	1	$e^2_{g\uparrow}a^1_{1g\uparrow}e^2_{u\uparrow}a^1_{1g\downarrow}e^1_{u\downarrow}e^0_{g\downarrow}$	3/2	$e^2_{u\uparrow}a^1_{1g\uparrow}a^1_{1g\downarrow}e^2_{g\uparrow}e^2_{g\downarrow}e^0_{u\downarrow}$	1
2−	$e^2_{u\uparrow}e^2_{u\downarrow}a^1_{1g\uparrow}e^0_{g\uparrow}e^0_{g\downarrow}a^0_{1g\downarrow}$	1/2	$e^2_{g\uparrow}a^1_{1g\uparrow}e^2_{u\uparrow}e^2_{u\downarrow}a^1_{1g\downarrow}e^0_{g\downarrow}$	1	$e^2_{u\uparrow}a^1_{1g\uparrow}a^1_{1g\downarrow}e^2_{g\uparrow}e^2_{g\downarrow}e^1_{u\downarrow}$	1/2
3−	$e^2_{u\uparrow}e^2_{u\downarrow}e^2_{g\uparrow}a^0_{1g\uparrow}a^0_{1g\downarrow}e^0_{g\downarrow}$	1	$e^2_{g\uparrow}e^2_{u\uparrow}e^2_{u\downarrow}a^1_{1g\uparrow}e^2_{g\downarrow}a^0_{1g\downarrow}$	1/2	$e^2_{u\uparrow}e^2_{u\downarrow}a^1_{1g\uparrow}a^1_{1g\downarrow}e^2_{g\uparrow}e^2_{g\downarrow}$	0
4−	$e^2_{u\uparrow}e^2_{u\downarrow}e^2_{g\uparrow}a^1_{1g\uparrow}e^0_{g\downarrow}a^0_{1g\downarrow}$	3/2	$e^2_{u\uparrow}e^2_{u\downarrow}a^1_{1g\uparrow}a^1_{1g\downarrow}e^2_{g\uparrow}e^2_{g\downarrow}$	0	——	—

centers introduce energy levels with t_2 and e irreducible representations in the band gap, with $t_{2\uparrow}$ and $t_{2\downarrow}$ states below the $e_\uparrow$ and $e_\downarrow$ ones. For an impurity with a $3d^n4s^2$ atomic configuration, those levels are filled with $(n+2)d$ electrons. The first possible transition energy is associated with the electronic initial and final configurations $t^0_{2\uparrow}t^0_{2\downarrow}e^0_\uparrow e^0_\downarrow \rightarrow t^1_{2\uparrow}t^0_{2\downarrow}e^0_\uparrow e^0_\downarrow$. It could be represented in a compact form as $t^0_2 \rightarrow t^1_2$, or just $[t^0_2/t^1_2]$ in Fig. 5. Those configurations are associated with the (3+/2+) and (4+/3+) transition states for the Sc_i and Ti_i impurities, respectively. After all the t_2 states are filled with increasing Fermi energy, the large energy difference for the $t^6_2e^0_\uparrow e^0_\downarrow \rightarrow t^6_2e^1_\uparrow e^0_\downarrow$ electronic configurations (or in compact form $e^0 \rightarrow e^1$) is associated with the crystal field splitting (Δ^i_{CF}), consistent with the model of Fig. 1. For all those centers it is observed that any transition state along the $3d$ series has a chemical trend to move from the upper half region of the band gap, in Sc, toward the valence band maximum, in Cu. Additionally, the crystal field splitting for the TM_i centers is considerably smaller than the respective splitting for the TM_s ones ($\Delta^i_{CF} \ll \Delta^s_{CF}$).

For the TM_{2V}, this model could be applied only to a few transition states, since the almost noninteracting divacancy-related energy levels and the $3d$-related ones lie in the same region of the band gap, as shown in Fig. 2. As mentioned earlier, the divacancy-related states (e_u) remain in the bottom of the band gap; the $3d$-related states ($e_g + a_{1g}$) move from the top of the gap in Sc toward the valence band in Cu. While some transition states are computed in association with electronic configurations filling the divacancy-related states, others are associated with filling the TM-related states. The transition energies associated with the TM_{2V} centers are presented in Fig. 6. The trends can be observed here for some TM impurities. On the other hand, the V, Fe, and Co are exceptions, since the highest occupied level in their neutral charge state has a $3d$-related character, as shown in Fig. 2. For those cases the electronic configurations are considerably richer, which are presented in Table II for several charge states. Therefore, Table II helps to assign the electronic configurations associated with the respective transitions. According to Fig. 6, in general, transition energies related to occupying the divacancy-related orbitals (e_u) are in the lower part of the band gap while transition states associated to occupying the $3d$-related states (e_g and a_{1g}) are mostly in the upper part of the band gap.

IV. SUMMARY

In summary, we have investigated the electronic properties and chemical trends of isolated $3d$ transition metal impurities in diamond. We have shown that impurities in the substitutional or double semivacancy centers have smaller formation energies than the isolated centers in the interstitial site. We have also shown that trends on transition energies, for any of the three sites, could only be rationalized if they were discussed in terms of the increasing occupation of $3d$-related states in the band gap. Such trends are consistent with what would be expected for transition metal impurities in other semiconductors in either isolated configurations[33,34] or forming complexes with other defects.[29,35]

ACKNOWLEDGMENTS

The authors acknowledge support from the Brazilian agencies CNPq and FAPESP. The calculations were performed in part using the computational facilities of CENAPAD and LCCA-CCE of the University of São Paulo.

[1]M. Schulz, Nature (London) **399**, 729 (1999).
[2]R. W. Keyes, Rep. Prog. Phys. **68**, 2701 (2005).
[3]V. V. Buniatyan and V. M. Aroutiounian, J. Phys. D **40**, 6355 (2007).
[4]Y. Gurbuz, O. Esame, I. Tekin, W. P. Kang, and J. L. Davidson, Solid State Electron. **49**, 1055 (2005).
[5]*Wide band gap Semiconductors: Fundamental Properties and Modern Photonic and Electronic Devices*, edited by K. Takahashi, A. Yoshikawa, and A. Sandhu (Springer, Berlin, 2007).
[6]M. V. G. Dutt, L. Childress, L. Jiang, E. Togan, J. Maze, F. Jelezko, A. S. Zibrov, P. R. Hemmer, and M. D. Lukin, Science **316**, 1312 (2007).

[7]A. A. Khajetoorians, B. Chilian, J. Wiebe, S. Schuwalow, F. Lechermann, and R. Wiesendanger, Nature (London) **467**, 1084 (2010).
[8]J. L. Hudgins, G. S. Simin, E. Santi, and M. A. Khan, IEEE Trans. Power Electron. **18**, 907 (2003).
[9]R. J. Nicholas, A. Mainwood, and L. Eaves, Philos. Trans. R. Soc. London, Ser. A **366**, 189 (2008).
[10]C. J. H. Wort and R. S. Balmer, Mater. Today **11**, 22 (2008).
[11]F. P. Bundy, H. T. Hall, H. M. Strong, and R. H. Wentorf, Nature (London) **176**, 51 (1955).
[12]A. Yelisseyev and H. Kanda, New Diamond Front. Carbon Technol. **17**, 127 (2007).
[13]R. Larico, J. F. Justo, W. V. M. Machado, and L. V. C. Assali, Phys. Rev. B **79**, 115202 (2009).
[14]A. T. Collins, Diamond Relat. Mater. **9**, 417 (2000).
[15]K. Iakoubovskii and A. T. Collins, J. Phys. Condens. Matter **16**, 6897 (2004).
[16]V. A. Nadolinny, J. M. Baker, O. P. Yuryeva, M. E. Newton, D. J. Twitchen, and Y. N. Palyanov, Appl. Magn. Reson. **28**, 365 (2005).
[17]D. J. Singh, *Planewaves, Pseudopotentials and the LAPW Method* (Kluwer Academic, Norwell, MA, 1994).
[18]P. Blaha, K. Schwarz, G. Madsen, D. Kvaniscka, and J. Luitz, in *WIEN2K, An Augmented Plane Wave Plus Local Orbitals Program for Calculating Crystal Properties*, edited by K. Schwarz (Technical Universität Wien, Austria, 2001).
[19]J. P. Perdew, K. Burke, and M. Ernzerhof, Phys. Rev. Lett. **77**, 3865 (1996).
[20]H. J. Monkhorst and J. D. Pack, Phys. Rev. B **13**, 5188 (1976).
[21]R. Larico, L. V. C. Assali, W. V. M. Machado, and J. F. Justo, Appl. Phys. Lett. **84**, 720 (2004).
[22]F. Ayres, L. V. C. Assali, W. V. M. Machado, and J. F. Justo, Appl. Phys. Lett. **88**, 11918 (2006).
[23]L. V. C. Assali, W. V. M. Machado, and J. F. Justo, Phys. Rev. B **69**, 155212 (2004).
[24]T. Mattila and A. Zunger, Phys. Rev. B **58**, 1367 (1998).
[25]P. J. Dean, E. C. Lightowlers, and D. R. Wright, Phys. Rev. **140**, A352 (1965).
[26]C. Stampfl, C. G. Van de Walle, D. Vogel, P. Kruger, and J. Pollmann, Phys. Rev. B **61**, R7846 (2000).
[27]T. V. Albu, A. B. Anderson, and J. C. Angus, J. Electrochem. Soc. **149**, E143 (2002).
[28]L. V. C. Assali, W. V. M. Machado, and J. F. Justo, Appl. Phys. Lett. **89**, 072102 (2006).
[29]L. V. C. Assali and J. F. Justo, Phys. Rev. B **58**, 3870 (1998).
[30]L. V. C. Assali, W. V. M. Machado, and J. F. Justo, Physica B **404**, 4515 (2009).
[31]T. Jungwirth, J. Sinova, J. Masek, K. Kucera, and A. H. MacDonald, Rev. Mod. Phys. **78**, 809 (2006).
[32]E. B. Lombardi, Diamond Relat. Mater. **17**, 1345 (2008).
[33]H. Raebiger, S. Lany, and A. Zunger, Phys. Rev. B **79**, 165202 (2009).
[34]A. Continenza, G. Profeta, and S. Picozzi, Phys. Rev. B **73**, 035212 (2006).
[35]S. Zhao, L. V. C. Assali, J. F. Justo, G. H. Gilmer, and L. C. Kimerling, J. Appl. Phys. **90**, 2744 (2001).